

Experimental and Numerical Analysis of Injection Molding of Ti-6Al-4V Powders for High-Performance Titanium Parts

DONGGUO LIN,¹ TAE GON KANG,^{2,4} JUN SAE HAN,¹
SEONG JIN PARK,^{1,9} SEONG TAEK CHUNG,³ and YOUNG-SAM KWON³

1.—Department of Mechanical Engineering, Pohang University of Science and Technology, 77 Cheongam-ro, Nam-gu, Pohang, Gyeongbuk 37673, Republic of Korea. 2.—School of Aerospace and Mechanical Engineering, Korea Aerospace University, 76 Hanggongdaehang-ro, Goyang-si, Gyeonggi-do 10540, Republic of Korea. 3.—CetaTech, Inc, GTIC 296-3, 102 Seonjingongwon-gil, Sacheon, Gyeongnam 52537, Republic of Korea. 4.—e-mail: tgkang@kau.ac.kr. 5.—e-mail: sj-park87@postech.ac.kr

Both experimental and numerical analysis of powder injection molding (PIM) of Ti-6Al-4V alloy were performed to prepare a defect-free high-performance Ti-6Al-4V part with low carbon/oxygen contents. The prepared feedstock was characterized with specific experiments to identify its viscosity, pressure–volume–temperature and thermal properties to simulate its injection molding process. A finite-element-based numerical scheme was employed to simulate the thermomechanical process during the injection molding. In addition, the injection molding, debinding, sintering and hot isostatic pressing processes were performed in sequence to prepare the PIMed parts. With optimized processing conditions, the PIMed Ti-6Al-4V part exhibits excellent physical and mechanical properties, showing a final density of 99.8%, tensile strength of 973 MPa and elongation of 16%.

INTRODUCTION

To manufacture titanium parts with complex shapes easily, powder injection molding of titanium and its alloy has become an important method, employed widely in a variety of areas including automotive, medical, airframe and accessory components.^{1–8} Although the entire titanium powder injection molding (Ti-PIM) process is similar to injection molding of other metal or ceramic powders, much more attention should be paid to carefully controlling the processing conditions.⁹ In Ti-PIM, large-sized titanium powders are usually used as powders in a feedstock to restrain their reactivity with oxygen, possibly leading to powder-binder separation during the injection molding process.^{10–12}

Simulating each process in PIM is an essential procedure to shorten the time to design and reduce the number of experiments.^{13–15} Many studies on the simulation of PIM have so far focused on the injection molding stage using the referenced or estimated material properties of a feedstock.^{16,17} These works are limited to conducting injection

molding experiments based on simulation results rather than performing the entire PIM process analysis and evaluating the quality of the final products. Barriere et al.¹⁶ conducted an experimental and numerical study on the optimal processing parameters for the injection molding of stainless steel 316L powders. The obtained parameters enabled them to prepare defect-free parts. However, there was little information on the characterization of material properties with an influence on the accuracy of simulation. Fang et al.¹⁷ also worked on the simulation of injection molding of a feedstock, focusing on powder-binder separation. They showed that the simulation is a powerful tool to optimize the injection molding conditions to fabricate defect-free parts. However, the results were not verified by experiments, limited only to the mold-filling stage.

To conduct reliable numerical simulations, as mentioned above, an accurate characterization of a feedstock is a prerequisite. Based on the simulation results, experiments should be conducted with optimized processing conditions to produce PIM parts with the desired mechanical properties and without any defects. As for the study concerning the

experiments and numerical simulations for Ti-PIM, especially including the characterization of material properties for a Ti feedstock, little work can be found in the literature. In this study, we experimentally and numerically investigated the PIM process of a titanium alloy feedstock. The feedstock was characterized systemically to obtain the rheologic and thermal properties to be used in numerical simulations. In addition, the entire PIM process was performed under optimized processing conditions to fabricate defect-free high-performance titanium parts.

EXPERIMENTAL

Materials

As starting materials, a spherical pre-alloyed Ti-6Al-4V powder of medium particle size (D_{50}) of 24.5 μm and a wax-polymer binder system consisting of paraffin wax (PW), polypropylene (PP), polyethylene (PE) and stearic acid (SA) were used. For detailed information on the powder and binder system, including the powder morphology, powder chemical composition, composition of the binder system and physical properties of each binder, we refer to our previous work.¹⁸

Feedstock Preparation and Characterization

The solid loading of the feedstock used in this work was 67 vol.%, based on its critical solid loading (71 vol.%) measured by torque rheometer experiments.¹⁸ Generally, the optimal solid loading is 2–5 vol.% points lower than the critical value.⁹ A 4 vol.% point lower value was determined to give sufficient flowability to the feedstock to increase its moldability. Mixing was conducted three times at 160°C using a twin-screw extruder enabling high shear mixing to obtain a homogeneous feedstock. The number of mixing operations was determined by observing the fluctuation of the viscosity of the feedstock at a specific shear rate using a plate-to-plate rheometer after each mixing.¹⁸ The material properties of the prepared feedstock, which have a significant influence on the success of injection molding, were characterized with a series of measurements. Material data related to the viscosity, specific heat, thermal conductivity, pressure–volume–temperature (PVT) relation and no-flow temperature were measured in sequence using a standard testing method for each material property.

Specimen Preparation and Characterization

In this section, we briefly address the way to prepare the PIMed titanium alloy parts. Using the injection molding conditions (injection temperature: 165°C, mold temperature: 50°C, injection pressure: 61 MPa, packing pressure: 58 MPa, packing time: 1.0 s, cooling time: 20 s), the feedstock was injection molded into ASTM E8 tensile test specimens. A two-step debinding process, consisting of solvent and

thermal debinding, was used to remove the binders resident inside the injection-molded parts. Solvent debinding is performed in a 50°C *n*-hexane bath for 12 h, followed by thermal debinding under a thermal cycle (from 25°C to 250°C: 2°C/min, holding: 3 h, from 250°C to 450°C: 1°C/min, holding: 3 h, from 450°C to 700°C: 1°C/min, holding: 1 h) in a tube-type furnace with a high-purity argon flow. Sintering was performed at 1250°C with the heating rate of 2°C/min and holding time of 2 h in a high-vacuum atmosphere. Finally, the sintered specimens were HIPed at 930°C and 100 MPa for 2 h to improve the density and mechanical strength. The mechanical properties of both sintered and HIPed samples were measured through a tensile test under the deformation speed of 2 mm/min. In addition, the chemical composition of the final product was measured using LECO combustion analysis.

MODELING AND NUMERICAL SCHEME FOR INJECTION MOLDING

In the filling stage, the flow is assumed to be incompressible. The governing equations for an incompressible generalized Newtonian fluid are as follows:

$$\nabla \cdot (2\mu\mathbf{D}) - \nabla p = \mathbf{0}, \quad (1)$$

$$\nabla \cdot \mathbf{u} = 0, \quad (2)$$

where μ is the viscosity, \mathbf{D} the rate-of-deformation tensor defined by $D = 1/2(\nabla\mathbf{u} + \nabla\mathbf{u}^T)$, p the pressure and \mathbf{u} the velocity. As for the boundary conditions, a prescribed velocity is imposed at the inlet. The no-slip condition is applied at the mold wall that is in contact with the fluid, but a free-slip condition is applied to the wall in the unfilled air region. At the vent, the no-slip condition is applied if the vent is in contact with the fluid, whereas a traction-free condition is applied if it is in the unfilled air region, as used in our previous studies.^{19,20} The heat transfer is modeled by the following energy equation,

$$\rho c_p \left(\frac{\partial T}{\partial t} + \mathbf{u} \cdot \nabla T \right) = \nabla \cdot (k\nabla T) + \mu \dot{\gamma}^2, \quad (3)$$

where T is the temperature, ρ the density, c_p the specific heat, t the time, k the thermal conductivity and $\dot{\gamma}$ the generalized shear rate defined by $\dot{\gamma} = \sqrt{2\mathbf{D} : \mathbf{D}}$. A fixed injection temperature is prescribed at the inlet and a constant temperature at the mold wall. During the cavity-filling process, the melt front is moving in time, which is treated by a scalar function called the pseudo-concentration function F , which is one in the completely filled region but zero in the unfilled region.¹⁹ The fluid-air interface is defined by an iso-surface where $F = 0.5$. By solving the advection equation for the concentration, given by

$$\frac{\partial F}{\partial t} + \mathbf{u} \cdot \nabla F = 0, \quad (4)$$

one can implicitly represent the moving melt front in time. Initially, F is set to zero in the unfilled domain. Since Eq. 4 is a pure advection equation, a boundary condition only at the inlet is needed, which is $F = 1$.

As for the viscosity of the feedstock, the Cross-WLF model is employed, given by

$$\mu(T, \dot{\gamma}) = \frac{\mu_0}{1 + \left[\frac{\mu_0 \dot{\gamma}}{\tau^*} \right]^{(1-n)}} \quad (5)$$

$$\mu_0 = D_1 \exp\left(\frac{A_1(T - T^*)}{A_2 + T - T^*}\right), \quad (6)$$

where μ_0 is the zero-shear-rate viscosity. The parameters in the viscosity model, n , τ^* , D_1 , A_1 and A_2 , are obtained by curve fitting of the experimental characterization.

A numerical scheme based on the finite element method (FEM) was employed to solve the flow and heat transfer in the filling stage of the PIM process. The computational domain is discretized by linear tetrahedral elements. A stabilized finite element formulation²¹ is used to solve the flow problems. The streamline-upwind/Petrov–Galerkin (SUPG) method²² is employed to solve the transport equation for the pseudo-concentration and the energy equations, preventing numerical oscillations in convection-dominant problems. For details on the finite element formulations, we refer to our previous works.^{19,20}

RESULTS AND DISCUSSION

Characteristics of Feedstock

First, we characterized the material properties of the prepared feedstock, which are essential to perform accurate injection molding simulations. Figure 1a shows the relationship between the shear rate and viscosity of the feedstock at the temperature ranging from 140°C to 180°C. German et al.⁹ suggested that the viscosity of the feedstock should be lower than 1000 Pa·s at the shear rate range between 100 s⁻¹ and 100,000 s⁻¹ to be successfully injection molded. As shown in Fig. 1a, this requirement holds for the prepared feedstock at the three temperatures, indicating that the feedstock has a good flowability to be injection molded. The experimental results were curve fitted with the Cross-WLF model (Eqs. 5 and 6). The fitted parameters of n , τ^* , D_1 , D_2 , A_1 and A_2 are 0.47, 9469 Pa, 8.6×10^9 Pa·s, 263 K, 22.6 K, and 51.6 K, respectively.

It is important to understand the states of the feedstock during the entire process of injection molding. Figure 1b shows the PVT diagram of the feedstock, describing the relationship between

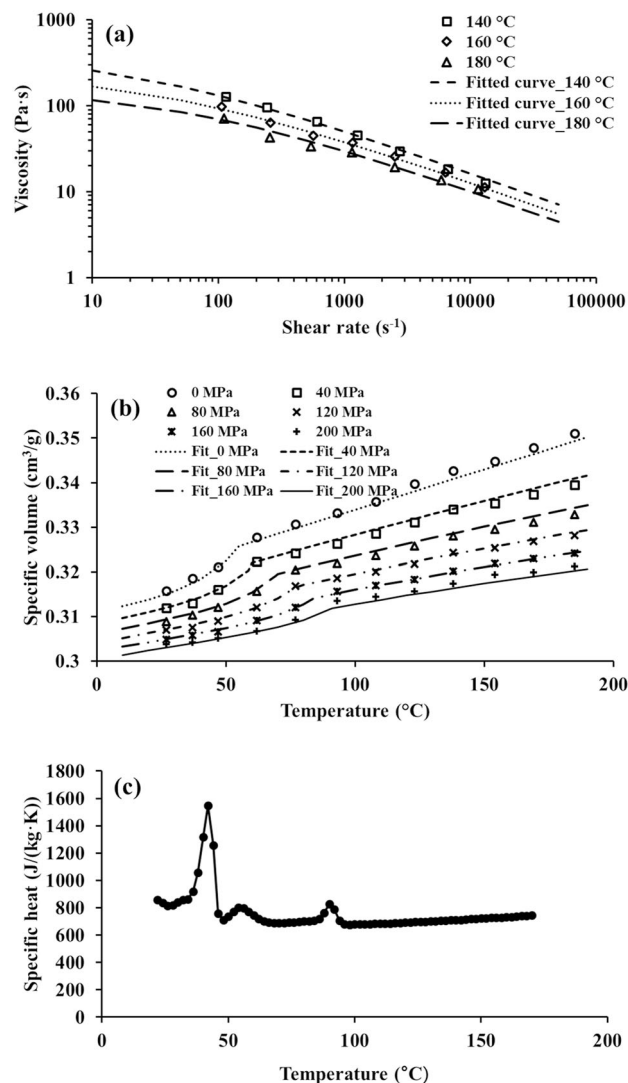


Fig. 1. Characteristics of prepared feedstock characterized through experiments. (a) Rheologic properties with the relationship between the shear rate and viscosity at different temperatures. (b) The PVT diagram showing the relationship between temperature and specific volume at different pressures. (c) Thermal property showing the relationships between temperature and specific heat.

temperature and specific volume at a pressure ranging from 0 MPa to 200 MPa. The transition temperature increases as the pressure increases. The density at the injection temperature and the typical injection pressure is used as an input parameter in injection molding filling simulation.

The thermal properties of the feedstock were also characterized experimentally. The specific heat of the feedstock was measured by a differential scanning calorimetry experiment at different temperatures ranging from 20°C to 180°C as shown in Fig. 1c. Three peaks appear at 42°C, 56°C and 90°C, representing the melting points of the binder components in the feedstock. In addition, the thermal conductivity of the feedstock at different temperatures was measured using a line-source method. At

the three temperatures, 150°C, 165°C, and 180°C, the feedstock has a thermal conductivity value of about 3.1 W/m K, 2.0 W/m K and 1.9 W/m K, respectively.

Simulation Results and Verification

Numerical simulations for the PIM filling stage were conducted using the numerical model presented in “Modeling and Numerical Scheme for Injection Molding” section. In this section, results for injection molding filling simulation of an ASTM E8 tensile test specimen will be introduced. Figure 2a shows the finite element mesh for the cavity of the specimen, discretized by 153,526 linear tetrahedral elements with 31,042 nodes. In simulation, the material properties of the Ti-6Al-4V feedstock presented in “Characteristics of Feedstock” section were used. As for processing conditions used in simulations, we used the same injection molding conditions as mentioned in “Specimen Preparation and Characterization” section. Although we conducted numerical simulations for the filling and post-filling stages, in this article, results for the filling stage will be presented. Figure 2b shows the distribution of fill time, the time required to fill a specific location in the cavity. At first, the melt flows into the cavity from the gate, and the flow is divided into two streams. In this case, the gate is located near the lower grip part (not the center of the specimen) to avoid defects that can be formed at the gauge area. The lower grip part near the gate is filled first. Then, the melts flow toward the gauge area and the upper grip part until the entire cavity is filled. To compare the numerical results with the experimental data, short-shot tests were performed. As depicted in Fig. 3, 17 snapshots were taken during the filling process. The two results show good agreement, demonstrating the accuracy of the measured material properties and numerical models used in the simulations.

Mechanical Properties of the Final Parts

The entire PIM process was carried out to determine the mechanical properties of the PIMed part. After preparing the green parts with optimized injection molding conditions, the solvent debinding, thermal debinding, sintering and HIP processes were carried out in sequence.

Referring to the online supplementary material, supplementary Fig. S-1 shows the solvent debinding curve of the green tensile test parts, illustrating that the PW binder can be removed after 12 h. The thermal debinding condition was optimized based on thermogravimetric (TG) experimental results as shown in supplementary Fig. S-2a. A very small amount of the remaining binders (PW and SA) and a large amount of the backbone binders (PP and PE) started to decompose around 200°C and 400°C, respectively. As the heating rates increase, the decomposition temperature of the backbone binders

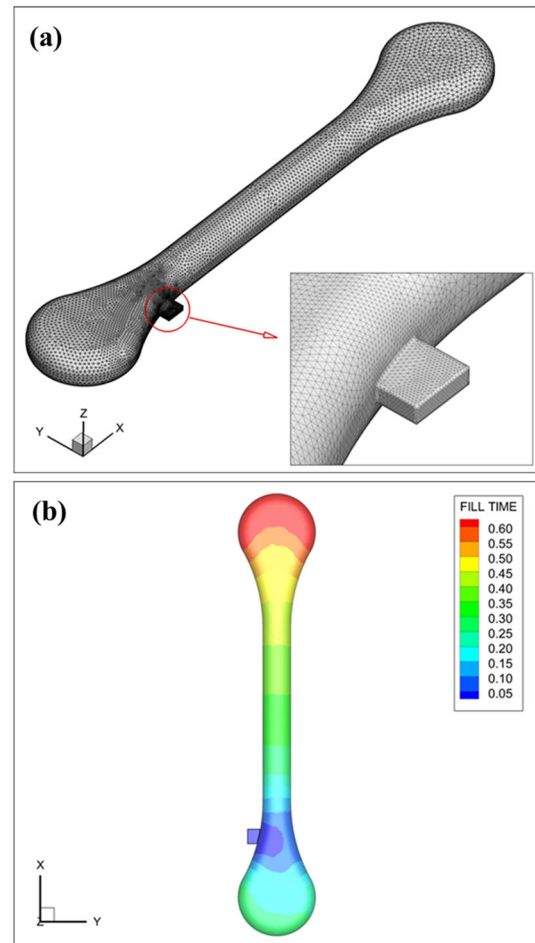


Fig. 2. Structural modeling and simulation result of injection molding. (a) FE mesh consisting of 153,526 tetrahedral elements with 31,042 nodes. (b) Contours of the fill time for the specimen geometry.

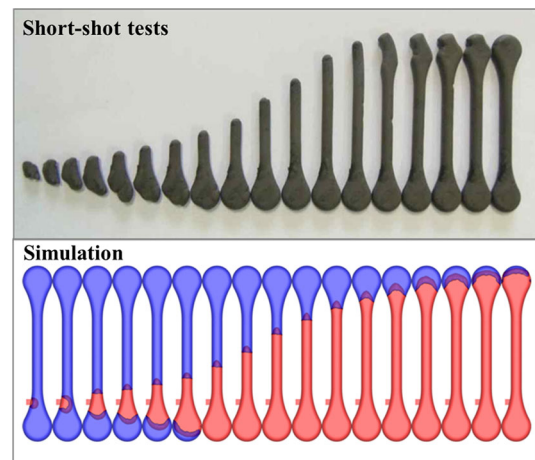


Fig. 3. Experiment and simulation results on short-shot tests of prepared Ti-6Al-4V feedstock.

is lagged. To analyze the binder decomposition behavior in more detail, the weight loss rate of binders at three heating rates was calculated, as shown in supplementary Fig. S-2b, which describes

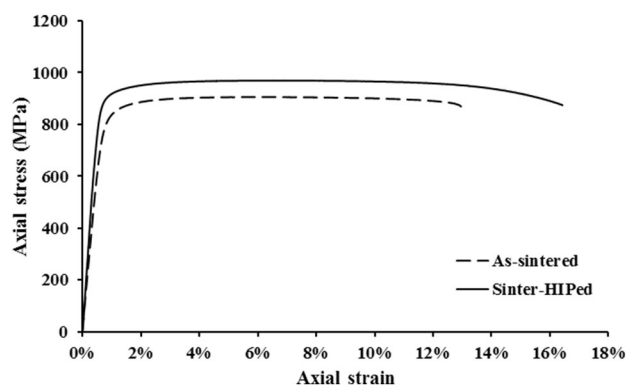


Fig. 4. Strain-stress curves of as-sintered and sinter-HIPed samples.

the rate of binder removal as a function of the temperature. The larger the heating rate is, the faster the weight loss, indicating that the binder removal occurs more rapidly. To avoid the defects caused by the fast binder removal, low heating rates are used. In addition, the holding temperature is set to 250°C and 450°C to completely remove the remaining PW, SA and backbone binders. At the final stage of thermal debinding, the samples were heated up to 700°C to pre-sinter the powders, providing the mechanical strength for the subsequent sintering process.

The processing conditions for sintering and HIP were also optimized through experiments and literature surveys. Figure 4 shows the strain-stress curve of as-sintered and sinter-HIPed samples. After sintering, the shrinkage of samples in the length direction was around 11%, showing the average relative density of 96.05%, tensile strength of 902 MPa, yield strength of 815 MPa and elongation of 13%. However, after the HIP process, the four values increased to 99.84%, 973 MPa, 902 MPa and 16%, showing reasonably good mechanical properties compared with those summarized in previous research.^{7,9} The increased mechanical properties are due to the relatively high solid-loading, defect-free molded samples and carefully optimized debinding and densification conditions, leading to quite low oxygen and carbon contents in the final densified samples. The oxygen and carbon contents in the final sinter-HIPed part were 0.20% and 0.09%, respectively, which are quite low values for PIMed titanium parts.

CONCLUDING REMARKS

In this work, the injection molding of Ti-6Al-4V powder and wax-polymer binder mixtures was both experimentally and numerically analyzed to optimize its injection molding conditions. The filling simulation results show good agreement with the experimental results, demonstrating the accuracy of the characterized feedstock properties and the validity of the numerical models. Defect-free Ti-

6Al-4V parts with high mechanical performance were successfully produced by a PIM process incorporating optimized processing conditions.

ACKNOWLEDGEMENT

This work was supported by the research project of the Civil Military Technology Cooperation Program and National Research Foundation of Korea (NRF) Grant funded by the Korea government (MSIT) (No. 2011-0030075).

ELECTRONIC SUPPLEMENTARY MATERIAL

The online version of this article (<https://doi.org/10.1007/s11837-018-2786-3>) contains supplementary material, which is available to authorized users.

REFERENCES

1. S.J. Park, Y. Wu, D.F. Heavey, X. Zou, G. Gai, and R.M. German, *Metall. Mater. Trans. A* 40A, 215 (2009).
2. S. Guo, X. Qu, X. He, T. Zhou, and B. Duan, *J. Mater. Process. Technol.* 173, 310 (2006).
3. J. Soyama, M. Oehring, T. Ebel, K.U. Kainer, and F. Pyczak, *JOM* 69, 676 (2017).
4. M. Qian and F.H. Froes, *Titanium Powder Metallurgy: Science, Technology and Applications*, 1st ed. (Waltham: Elsevier, 2015), pp. 337–360.
5. R.M. German and A. Bose, *Injection Molding of Metals and Ceramics*, 1st ed. (New Jersey: Metal Power Industries Federation, 1997), pp. 25–81.
6. T. Ebel, O.M. Ferri, W. Limberg, F.-P. Schimansky, and H.-Z. Geesthacht, *Adv. Powder. Metall. Part. Mater.* 1, 45 (2011).
7. A. Dehghan-Manshadi, M.J. Birmingham, M.S. Dargusch, D.H. StJohn, and M. Qian, *Powder Technol.* 319, 289 (2013).
8. A. Dehghan-Manshadi, D. StJohn, M. Dargusch, Y. Chen, J.F. Sun, and M. Qian, *J. Manuf. Process.* 31, 416 (2018).
9. R.M. German, *Materials* 6, 3641 (2013).
10. A. Mannschatz, S. Hohn, and T. Moritz, *J. Eur. Ceram. Soc.* 30, 2827 (2010).
11. T.S. Shivashankar, R.K. Enneti, S.J. Park, R.M. German, and S.V. Atre, *Powder Technol.* 243, 79 (2013).
12. H.O. Gulsoy, N. Gulsoy, and R. Calisici, *Bio-Med. Mater. Eng.* 24, 1861 (2014).
13. D.F. Heaney, *Handbook of Metal Injection Molding*, 1st ed. (Cambridge: Woodhead Publishing Limited, 2012), pp. 197–231.
14. G. Aggarwal, S.J. Park, and I. Smid, *Int. J. Refract. Met. Hard Mater.* 24, 253 (2006).
15. S. Ahn, S.T. Chung, S.V. Atre, S.J. Park, and R.M. German, *Powder Metall.* 51, 318 (2008).
16. Th. Barriere, B. Liu, and J.C. Gelin, *J. Mater. Process. Technol.* 143–144, 636 (2003).
17. W. Fang, X. He, R. Zhang, S. Yang, and X. Qu, *Powder Technol.* 256, 367 (2014).
18. D. Lin, S.T. Chung, Y.S. Kwon, and S.J. Park, *J. Mech. Sci. Technol.* 30, 1859 (2016).
19. T.G. Kang and T.H. Kwon, *Int. Polym. Proc.* 22, 266 (2007).
20. J.-Y. Ho, J.M. Park, T.G. Kang, and S.J. Park, *Polym. Eng. Sci.* 52, 901 (2012).
21. L.P. Franca, S.L. Frey, and T.J.R. Hughes, *Comput. Methods Appl. Mech. Eng.* 99, 209 (1992).
22. A.N. Brooks and T.J.R. Hughes, *Comput. Methods Appl. Mech. Eng.* 32, 199 (1982).